

PAPER • OPEN ACCESS

# Hot corrosion behaviour of constant and pulsed current welded Hastelloy X in $\text{Na}_2\text{SO}_4$ , $\text{V}_2\text{O}_5$ , and NaCl salt mixture at 900 °C

To cite this article: M Sathishkumar *et al* 2022 *Mater. Res. Express* 9 020008

View the [article online](#) for updates and enhancements.

You may also like

- [Hot corrosion behaviour of continuous and pulsed current gas tungsten arc welded Hastelloy X in different molten salts environment](#)  
M Sathishkumar and M Manikandan
- [High Temperature Corrosion studies on Pulsed Current Gas Tungsten Arc Welded Alloy C-276 in Molten Salt Environment](#)  
M Manikandan, M Arivarasu, N Arivazhagan *et al.*
- [Influence of filler wires and high velocity oxygen fuel coating on the structural properties of Inconel 600 and Nickel alloy 800 HT dissimilar joints using autogenous cold metal transfer welding](#)  
P S P Shankarganesh and R Selvabharathi



The Electrochemical Society  
Advancing solid state & electrochemical science & technology

242nd ECS Meeting

Oct 9 – 13, 2022 • Atlanta, GA, US

Abstract submission deadline: **April 8, 2022**

Connect. Engage. Champion. Empower. Accelerate.

**MOVE SCIENCE FORWARD**



Submit your abstract



# Materials Research Express



## PAPER

# Hot corrosion behaviour of constant and pulsed current welded Hastelloy X in $\text{Na}_2\text{SO}_4$ , $\text{V}_2\text{O}_5$ , and $\text{NaCl}$ salt mixture at $900^\circ\text{C}$

### OPEN ACCESS

#### RECEIVED

20 November 2021

#### REVISED

7 February 2022

#### ACCEPTED FOR PUBLICATION

9 February 2022

#### PUBLISHED

28 February 2022

Original content from this work may be used under the terms of the [Creative Commons Attribution 4.0 licence](#).

Any further distribution of this work must maintain attribution to the author(s) and the title of the work, journal citation and DOI.



M Sathishkumar<sup>1</sup> , M Manikandan<sup>2</sup> , N Arivazhagan<sup>2</sup>, B Arulmurugan<sup>3</sup> , Senthil Kumaran Selvaraj<sup>2</sup> , M Vignesh<sup>4</sup> , S Rajakumar<sup>5</sup> and S Rajkumar<sup>6,\*</sup>

<sup>1</sup> Department of Mechanical Engineering, Amrita School of Engineering, Amrita Vishwa Vidyapeetham, Chennai, India

<sup>2</sup> School of Mechanical Engineering, Vellore Institute of Technology, Vellore, India

<sup>3</sup> Department of Mechanical Engineering, KPR Institute of Engineering & Technology, Coimbatore, India

<sup>4</sup> Department of Mechanical Engineering, Sri Venkateswara College of Engineering, Sriperumbudur, 602117, Tamil Nadu, India

<sup>5</sup> Centre for Materials Joining and Research, Department of Manufacturing Engineering, Annamalai University, Chidambaram, India

<sup>6</sup> Department of Mechanical Engineering, Faculty of Manufacturing, Institute of Technology, Hawassa University, Hawassa, Ethiopia

\* Author to whom any correspondence should be addressed.

E-mail: [mano.manikandan@gmail.com](mailto:mano.manikandan@gmail.com) and [rajkumar@hu.edu.et](mailto:rajkumar@hu.edu.et)

**Keywords:** hastelloy X, C263, ERNiCr-3 fillers, pulsed current, parabolic constant, spallation and cracking

## Abstract

The high-temperature corrosion behavior of constant current gas tungsten arc (GTA) and pulsed current gas tungsten arc (PCGTA) welded Hastelloy X with different filler wires (C263 and ERNiCr-3) are studied for 50 cycles at  $900^\circ\text{C}$ . Molten salt I (MS I) ( $75\% \text{Na}_2\text{SO}_4 + 25\% \text{V}_2\text{O}_5$ ) and molten salt II (MS II) ( $75\% \text{Na}_2\text{SO}_4 + 20\% \text{V}_2\text{O}_5 + 5\% \text{NaCl}$ ) were coated on the welded specimens. MS II coated substrate shows the highest weight gain than MS I with a parabolic constant for GTA ERNiCr-3 as  $21.440 \times 10^{-6} \text{mg}^2/(\text{cm}^4 \cdot \text{s})$ . Whereas PCGTA C263 welded sample with MS I, revealed parabolic constant (lowest) of  $0.008 \times 10^{-6} \text{mg}^2/(\text{cm}^4 \cdot \text{s})$ . Based on the results, an increasing pattern of hot corrosion resistance of substrates is arranged as  $\text{GTA ERNiCr-3} < \text{GTA C263} < \text{PCGTA C263} < \text{PCGTA ERNiCr-3}$ . PCGTA shows more refined grains, higher grain boundary volume, better corrosion resistance, and more protective phases like  $\text{Cr}_2\text{O}_3$ ,  $\text{NiO}$ ,  $\text{NiCr}_2\text{O}_4$ ,  $\text{CoCr}_2\text{O}_4$ ,  $\text{Al}_2\text{O}_3$ ,  $\text{NiFe}_2\text{O}_4$ ,  $\text{NbO}$  than GTA weldment. But phases such as  $\text{Fe}_2\text{O}_3$ ,  $\text{MoO}_3$ , and  $\text{Cr}_2\text{S}_3$  (non-protective phases) decrease corrosion resistance due to acid fluxing of alloying elements that promote the oxide scale exfoliation, spallation, chipping, and cracking. This study observed that PCGTA with C263 filler in MS I and MS II environment provides good corrosion resistance at high temperatures.

## 1. Introduction

The aerospace industry's tremendous development creates a demand for operating materials because of a continuous increase in combustion chamber temperature for improving performance. It needs the material to withstand a very high temperature without degrading its strength and corrosion resistance [1–4]. Hastelloy X is the best candidate material for this kind of application with Nickel as a base element with other major elements like Mo, Fe, Cr. Solid strengthening mechanism is used to strengthen the material, and it withstands properties at high temperatures up to  $1200^\circ\text{C}$  [5–8]. It is used in afterburner, gas-cooled reactor, thrust reverser [9], and mainly in combustion chamber parts of aerospace components. Sometimes, the poor-quality fuel used during the combustion process causes impurities like V, S, Cl & Na [10]. These impurity elements form MS compounds like  $\text{NaCl}$ ,  $\text{V}_2\text{O}_5$ , and  $\text{Na}_2\text{SO}_4$ , coated on the substrate. These salts reduce the life of the substrate during high-temperature conditions.

The low melting eutectic salts are formed from  $\text{Na}_2\text{SO}_4$ ,  $\text{V}_2\text{O}_5$  &  $\text{NaCl}$  blends at above  $650^\circ\text{C}$ . These eutectic salts increase the reduction and oxidation reaction when operated at an elevated temperature. There are two forms of hot corrosion: Type II ( $600^\circ\text{C}$  to  $800^\circ\text{C}$ ) and Type I ( $800^\circ\text{C}$  to  $950^\circ\text{C}$ ). The combustion chamber parts made of Hastelloy X material are operated at  $900^\circ\text{C}$  [10, 11] temperature. In the combustion chamber and

**Table 1.** Chemical composition of ERNiCr-3 filler wire, C263 & Hastelloy X.

Material & filler wires	Chemical composition (wt %)													
	Cr	Fe	Mo	Co	Si	Mn	Nb	Ti	C	Cu	Al	W	S	Ni
Hastelloy X	22.3	18.1	9.16	0.87	0.26	0.24	—	—	0.05	—	—	0.20	—	Bal
ERNiCr-3	18.2	3.0	—	0.12	0.50	2.50	2.0	0.75	0.10	—	—	—	0.02	Bal
C263	21.0	0.70	6.10	21.0	—	0.60	—	2.40	0.08	0.50	0.60	—	—	Bal

aerospace components, the Type I hot corrosion exhibits a vital [12], and hence it is considered for the present work.

Hot corrosion performance of gas turbine components made of Inconel 738LC coated with high activity Cr-aluminite [13] is investigated in different salts environment like, 25% V<sub>2</sub>O<sub>5</sub> + 75% Na<sub>2</sub>SO<sub>4</sub>, Na<sub>2</sub>SO<sub>4</sub>, 5% NaCl + 20% V<sub>2</sub>O<sub>5</sub> + 75% Na<sub>2</sub>SO<sub>4</sub> for 150 h and 300 h. The authors concluded that molten salts with NaCl possess a higher corrosion rate than the other two salts, and it exhibits cauliflower-like, plate-like, and broken plate-like structures. Fu guangyan *et al* [14] studied hot corrosion behaviour of pure Ni, Ni + 10% Cr, Ni + 10% Cr + 5% Al alloy in NaCl + Na<sub>2</sub>SO<sub>4</sub> molten salt mixture at 900 °C. The presence of Cr and Al in the Nickel-based alloy reduces the corrosion rate than pure Ni. Also, the presence of NaCl causes loose and porous particles.

Inconel 718 and Hastelloy coated by Alumina—Titania are investigated for the high-temperature behavior [15] for 50 h at 1000 °C. The authors concluded that the FeO scale formation on the thermally coated substrate started spalling due to repeated thermal cycles for a prolonged period. The Hastelloy has also shown less weight gain, low porosity, micro-cracks, and better corrosion resistance with respect to the Inconel 718. The authors recommended the Hastelloy materials for high-temperature applications over Inconel 718.

Surface modification of Inconel 718 alloy [16] was investigated in molten salts (100% NaCl, 10% V<sub>2</sub>O<sub>5</sub> + 15% NaCl + 75% Na<sub>2</sub>SO<sub>4</sub>) environment at 700 °C after nickel aluminide coating by ultrasonic shot peening and pack aluminizing method. The authors concluded that the nickel aluminide-coated samples showed better corrosion resistance, while ultrasonic shot peened samples revealed the worst corrosion resistance with respect to uncoated samples. The change in the surface activity of elements in Inconel 718 during the ultrasonic shot peening process affects the corrosion resistance.

Superni 601, 600, and 75 are coated with Ni-20Cr at 900 °C in the air environment [17] and studied for its hot corrosion behavior. A parabolic corrosion rate was observed in all the samples after 50 h by thermogravimetric analysis. NiO, NiCr<sub>2</sub>O<sub>4</sub>, Cr<sub>2</sub>O<sub>3</sub> phases are found, and spallation-free coating is achieved. Choi *et al* [16] investigated the effects of a bond coat (NiCrAlY) and topcoat (ZrO<sub>2</sub>–8% Y<sub>2</sub>O<sub>3</sub>) on Hastelloy X by a plasma spray technique. Authors revealed that the substrate bond strength and fatigue life increase with decreased coating residual stress and thickness.

Hari *et al* [18] studied hot corrosion propensity at 700 °C of alloy 617 used in the ultra-supercritical power plant. The authors coated the material with a molten salt mixture of Na<sub>2</sub>SO<sub>4</sub>, K<sub>2</sub>SO<sub>4</sub>, Fe<sub>2</sub>O<sub>3</sub>, SiO<sub>2</sub>, Al<sub>2</sub>O<sub>3</sub> and tested the coated material in a gas mixture environment and air environment. The sulfidation reaction occurs in both internal and external layers of the substrate in a gas mixture environment, and no such reactions occur in the air environment. Karimi *et al* [19] studied the top and bond coat remelting on Hastelloy X using GTA welding. The authors concluded that the three-time remelting using GTA welding revealed the best corrosion resistance compared to one-time remelting.

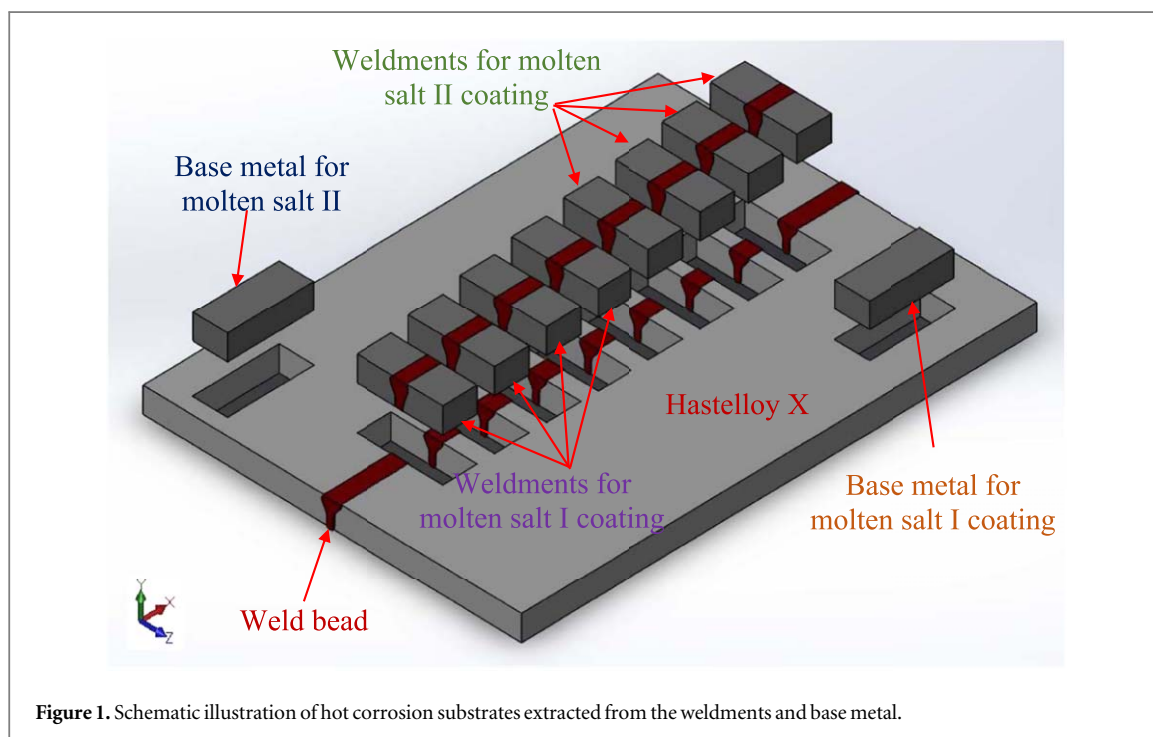
Hastelloy X's carburization kinetics in the CH<sub>4</sub> environment [20] was investigated at 1000 °C and 800 °C. The development of (Cr, Mo)<sub>23</sub>C<sub>6</sub>, (Cr, Mo)<sub>3</sub>C<sub>2</sub>, (Cr, Mo)<sub>7</sub>C<sub>3</sub>, carbide precipitates were observed on both outer and inner side parts. The internal carburization kinetics follows the parabolic rate law. Min Liu *et al* [21] studied Inconel 600, Hastelloy C276, and Hastelloy X in the molten fluoride environment at 750 °C. The results indicated that the Hastelloy C276 provided better corrosion resistance than Hastelloy X and Inconel 600 due to more Mo and low Cr content.

In a nitrogen gas environment, Yan Wang *et al* [22] studied Ni–Cr–Al–Fe alloy for its oxidation mechanism in the 850 °C to 1000 °C temperature range. The oxidized substrate reveals the presence of NiO, Al<sub>2</sub>O<sub>3</sub>, NiCr<sub>2</sub>O<sub>4</sub>, and Cr<sub>2</sub>O<sub>3</sub>. During the initial stages, the gamma prime phase favors the formation of these oxides. Sreenivasulu *et al* [22, 23] investigated the corrosion behavior of Nimonic 80A coated with metallic powder through air plasma and HVOF technique in 40% + 60% of Na<sub>2</sub>SO<sub>4</sub> + V<sub>2</sub>O<sub>5</sub> MS environment and air environment for 50 h at 900 °C. The authors concluded that spinel oxides and Cr<sub>2</sub>O<sub>3</sub> enhance corrosion resistance, whereas the MoO<sub>3</sub> decreases the corrosion resistance at the prescribed condition.

From the above literature, it has been clear that only minimal literature is reported on the oxidation behavior of welded Hastelloy X at a higher temperature. The substrate's salt mixture (NaCl, V<sub>2</sub>O<sub>5</sub>, and Na<sub>2</sub>SO<sub>4</sub>) reduces the corrosion resistance. In the present work, the corrosion behavior of Hastelloy X welded with GTA and

**Table 2.** Welding process conditions.

Welding method	Name of pass	Voltage in V	Speed of welding (mm s) <sup>-1</sup>	Heat supply (kJ mm) <sup>-1</sup>	Total heat supply (kJ mm) <sup>-1</sup>
GTA with C263 filler	Root	11.7	1.06	0.93	3.63
	1st	11.7	1.13	0.87	
	2nd	11.7	1.09	0.90	
	3rd	11.7	1.05	0.93	
PCGTA with C263 filler	Root	9.6	0.83	0.73	3.11
	1st	9.6	0.71	0.85	
	2nd	9.6	0.80	0.76	
	3rd	9.6	0.78	0.77	
GTA with ERNiCr-3 filler	Root	11.4	1.10	0.87	3.48
	1st	11.4	0.99	0.97	
	2nd	11.4	1.18	0.81	
	3rd	11.4	1.16	0.83	
PCGTA with ERNiCr-3 filler	Root	9.4	0.80	0.74	3.08
	1st	9.4	0.78	0.76	
	2nd	9.4	0.69	0.86	
	3rd	9.4	0.82	0.72	

**Figure 1.** Schematic illustration of hot corrosion substrates extracted from the weldments and base metal.

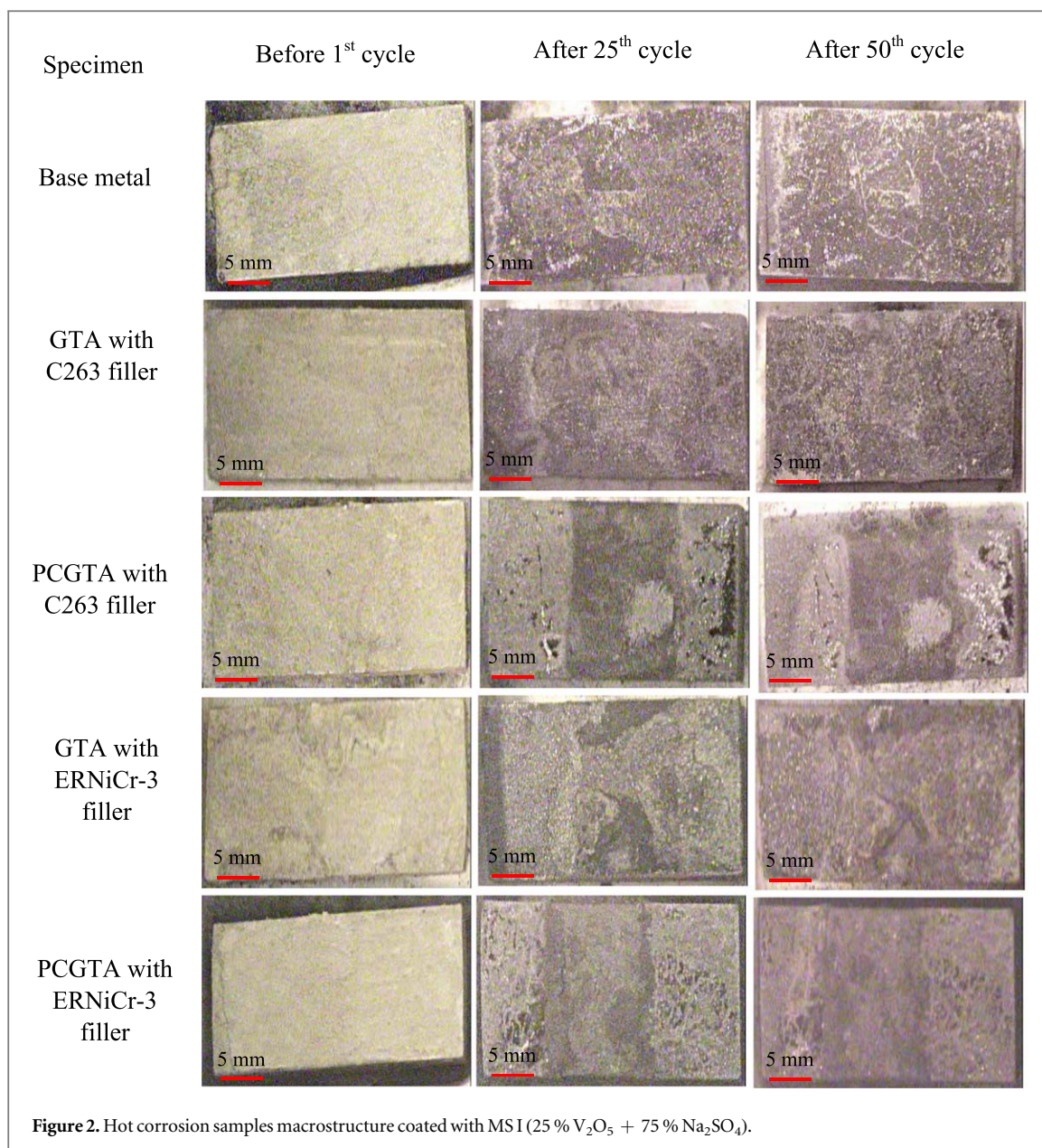
PCGTA technique at high temperature using C263 and ERNiCr-3 filler wire in two different molten salts 25%  $V_2O_5$  + 75%  $Na_2SO_4$ , 5%  $NaCl$  + 20%  $V_2O_5$  + 75%  $Na_2SO_4$ , is studied for 250 h at 900 °C.

## 2. Experimental steps

### 2.1. Hastelloy X

The base material received in solution-treated conditions consists of Mo, Fe, Cr, and Ni elements. The chemical composition of base material and filler wires (C263 & ERNiCr-3) are given in table 1. The received material is cut into 170 mm × 55 mm × 7 mm size, and its substrate is cleaned using the acid pickling technique and acetone. The edge preparation is done with 2 mm root gap specifications and a 30° bevel angle on the base material to finish the V-groove profile [24–27].



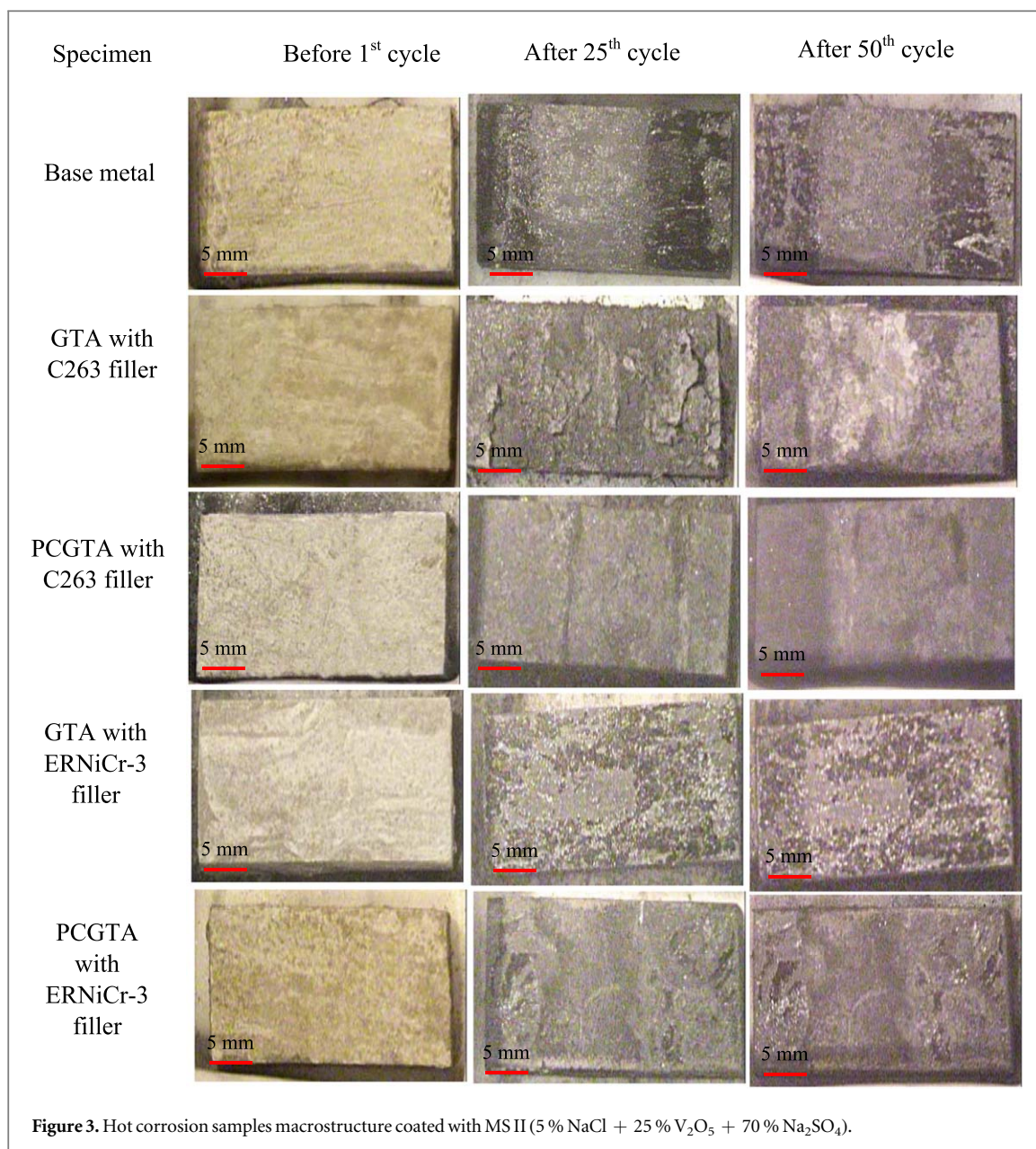


## 2.2. Welding on Hastelloy X

The PCGTA and GTA welding was done on the substrate material with two filler wires, C263 and ERNiCr-3. The process conditions utilized for welding are given in table 2. The welding was conducted by adopting the following conditions: application of argon shielding gas at 15 l min<sup>-1</sup>, filler wire diameter of 1.2 mm, tungsten electrode, standoff distance of 2 mm, 60 A of base current ( $I_{bc}$ ), 120 A of peak current ( $I_{pc}$ ), 120 A of continuous current ( $I_{cc}$ ), pulse frequency of 6 Hz and welding efficiency of 70% [8]. The heat input utilized during welding is displayed in table 2, and the full penetration is obtained in four passes. The welded substrate was tested by visual observation and radiography testing, which show no cracks and porosity in the weldment of both GTA and PCGTA. The samples for hot corrosion testing are then extracted from the weldment with a dimension of 25 mm × 10 mm × 7 mm (figure 1).

## 2.3. Hot corrosion experiment

The samples for hot corrosion were preheated for 2 h at 200 °C to eradicate the impurities, moisture from the substrate surface, and the uniform application of molten salts all over the surface. The MSI (25% V<sub>2</sub>O<sub>5</sub> + 75% Na<sub>2</sub>SO<sub>4</sub>) was mixed with acetone to make a slurry, and it was uniformly applied on all six surfaces. For moisture and impurities removal of coated samples, it was heated at 200 °C in the tubular furnace for 2 h. The above steps are followed until a uniform coating is obtained on the substrate surface between 3 mg mm<sup>-2</sup> to 5 mg mm<sup>-2</sup>. Similar measures have been observed for coating MSI II (5% NaCl + 20% V<sub>2</sub>O<sub>5</sub> + 75% Na<sub>2</sub>SO<sub>4</sub>) on the substrate surface. The specimens are introduced into the furnace in an alumina boat for 50 cycles at 900 °C. Each



cycle has 5 h of heating in the furnace and then air cooling for 40 min to attain room temperature. The specimens were then weighed using a weighing machine to identify the weight gain or loss due to oxidation of the surface after each cycle. Then the samples were kept back into the furnace for the next cycle, followed until the 50th cycle.

#### 2.4. Metallography analysis

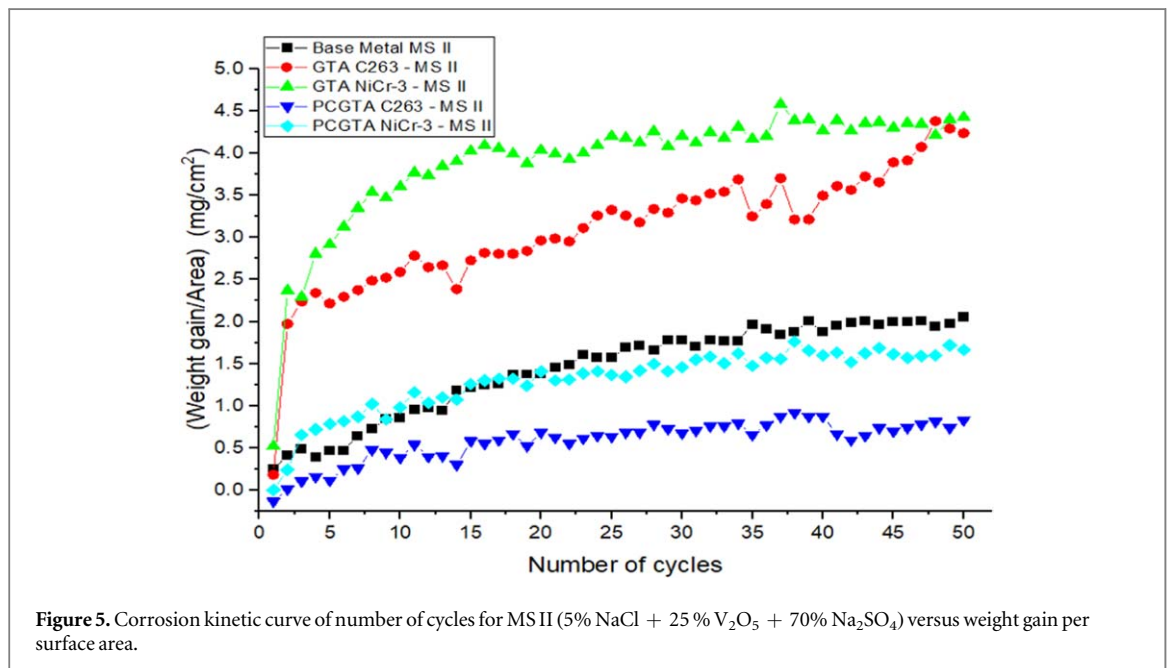
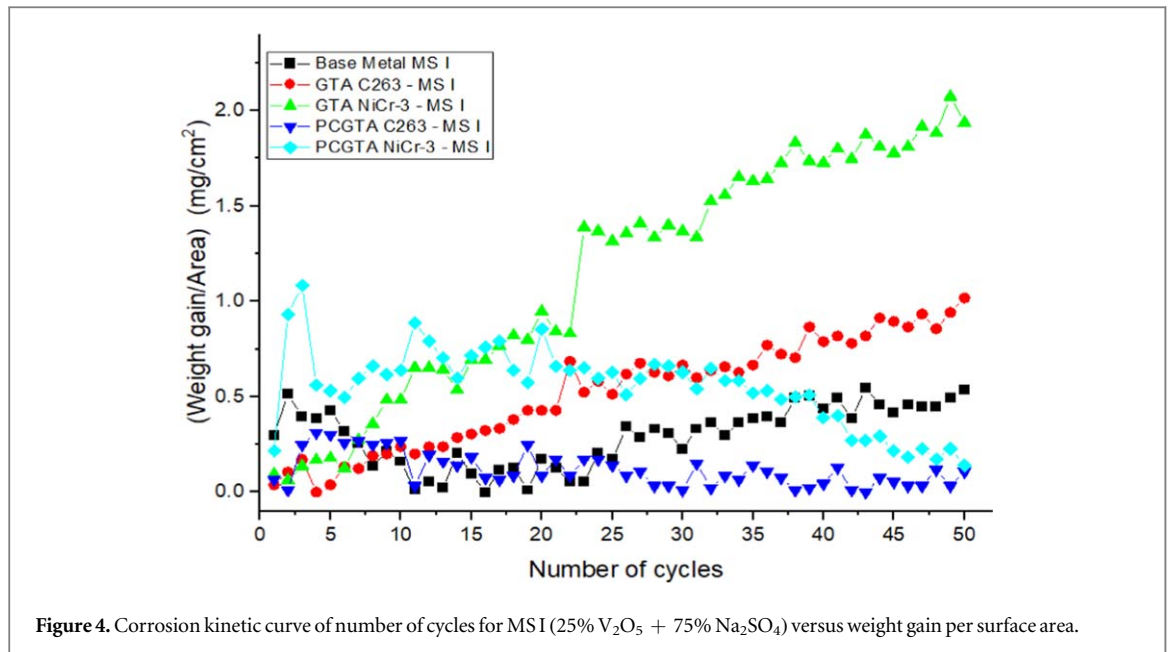
The residual salt on the substrate was removed by cleaning with distilled water. Scanning Electron Microscope (SEM) with Energy dispersive spectroscopy (EDS) attachment (Make: ZEISS EVO 18) was used to identify the chemical compositions and surface morphology [28–31]. The x-ray Diffraction (XRD) analysis (BRUKER D8 Advance) provided the substrate phases due to oxidation and reduction reaction.

### 3. Results and discussion

#### 3.1. Visual examination

The surface morphology of the welded substrate after each cycle was captured with an optical macroscope. Figure 2 and 3 display the MS I and MS II coated weldment images before the 1st cycle, after 25th and 50th cycles. The continuous changes in substrate colors after each cycle depict hot corrosion. After the 5th cycle, chipping and spalling occur in most of the substrates, and it keeps increasing till the 50th cycle. At the beginning of the





cycle, MS I coated substrate revealed a light greenish color, whereas MS II showed a light yellowish color. The substrate active elements enhance the rate of corrosion rapidly during the initial few cycles, and then it increases gradually until the 50th cycle [22]. In the GTA weldment of C263 and ERNiCr-3 fillers coated with MS I, during the 2nd cycle, the substrate color changes to light grey from light greenish and then to a dark grey color. Spalling and chipping start from the 6th cycle, continuing until the final cycle. A similar color change is found for PCGTA weldments of C263 and ERNiCr-3 filler, but very little spalling and chipping of the substrate are observed. The GTA weldment made with C263 and ERNiCr-3 fillers of the MS II coated substrate indicates the change of color from a light yellow to a light grey after the 2nd cycle after the 5th cycle gets changed to dark grey color, and it remains the same till 50th cycle. The PCGTA weldment with MS II displays similar color changes, but a small amount of chipping and spalling occurs.

### 3.2. Corrosion kinetics

The high-temperature corrosion kinetics (number of cycles vs. weight gain per unit area) with MS I and MS II coating on GTA and PCGTA weldment is illustrated in figures 4 and 5. The thermogravimetric analysis revealed that the MS I have shown a lesser weight gain per unit area than MS II for both the weldments. The MS I coated substrate offers better corrosion resistance when compared to MS II for the given condition. The absence of

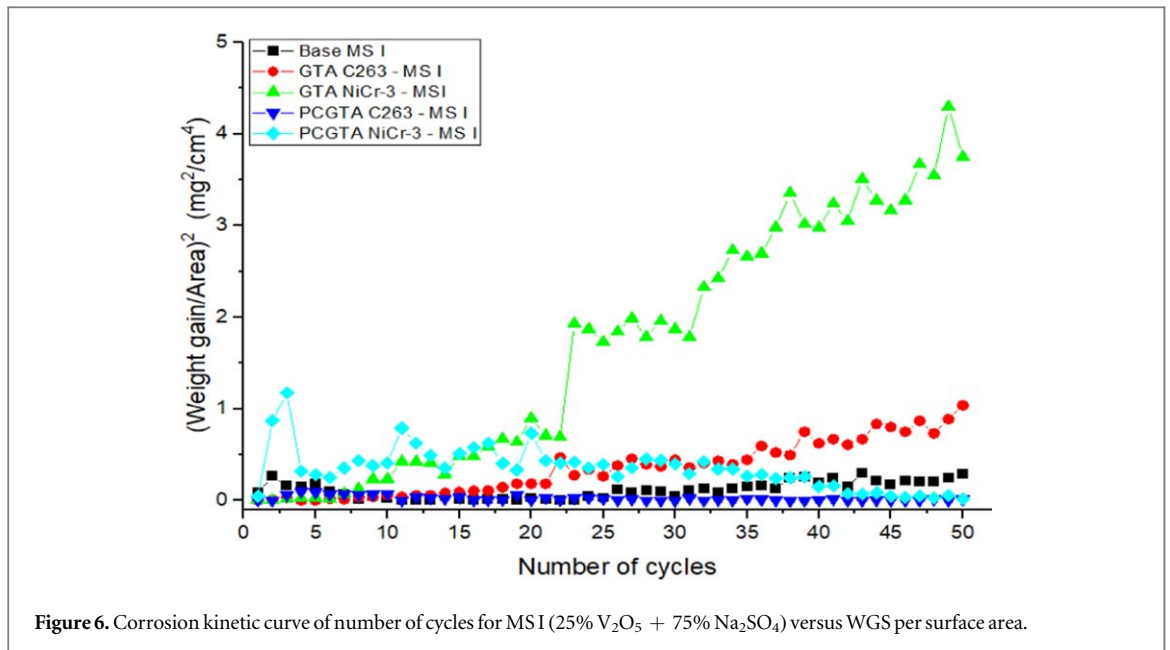


Figure 6. Corrosion kinetic curve of number of cycles for MSI (25% V<sub>2</sub>O<sub>5</sub> + 75% Na<sub>2</sub>SO<sub>4</sub>) versus WGS per surface area.

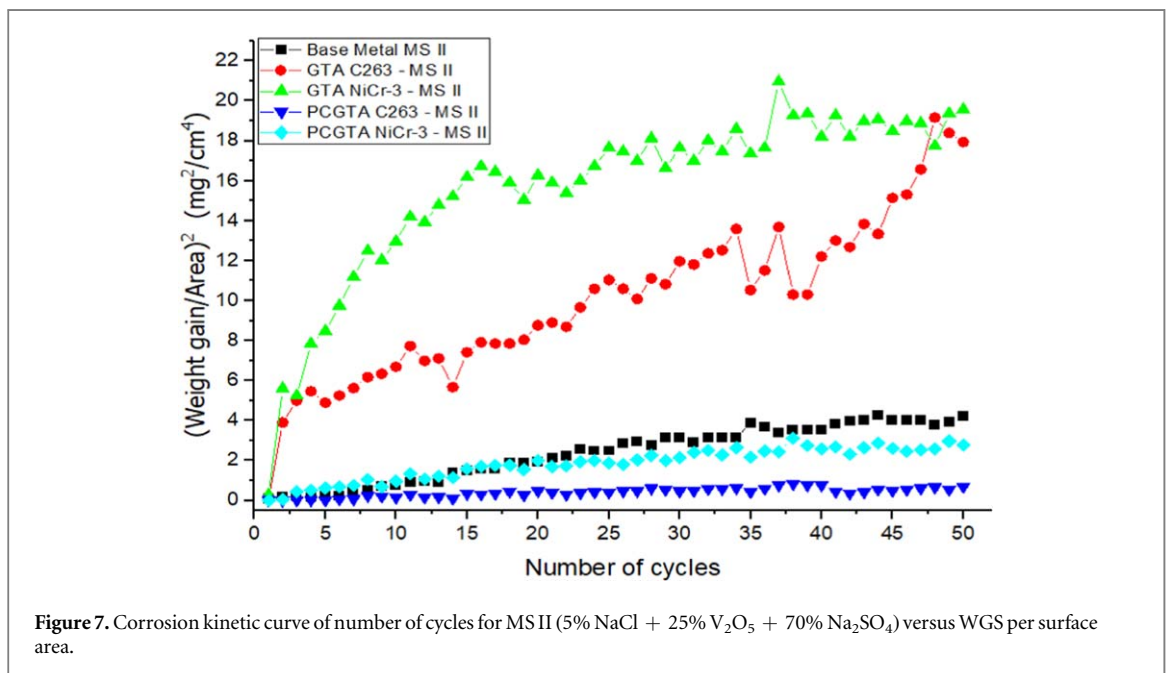
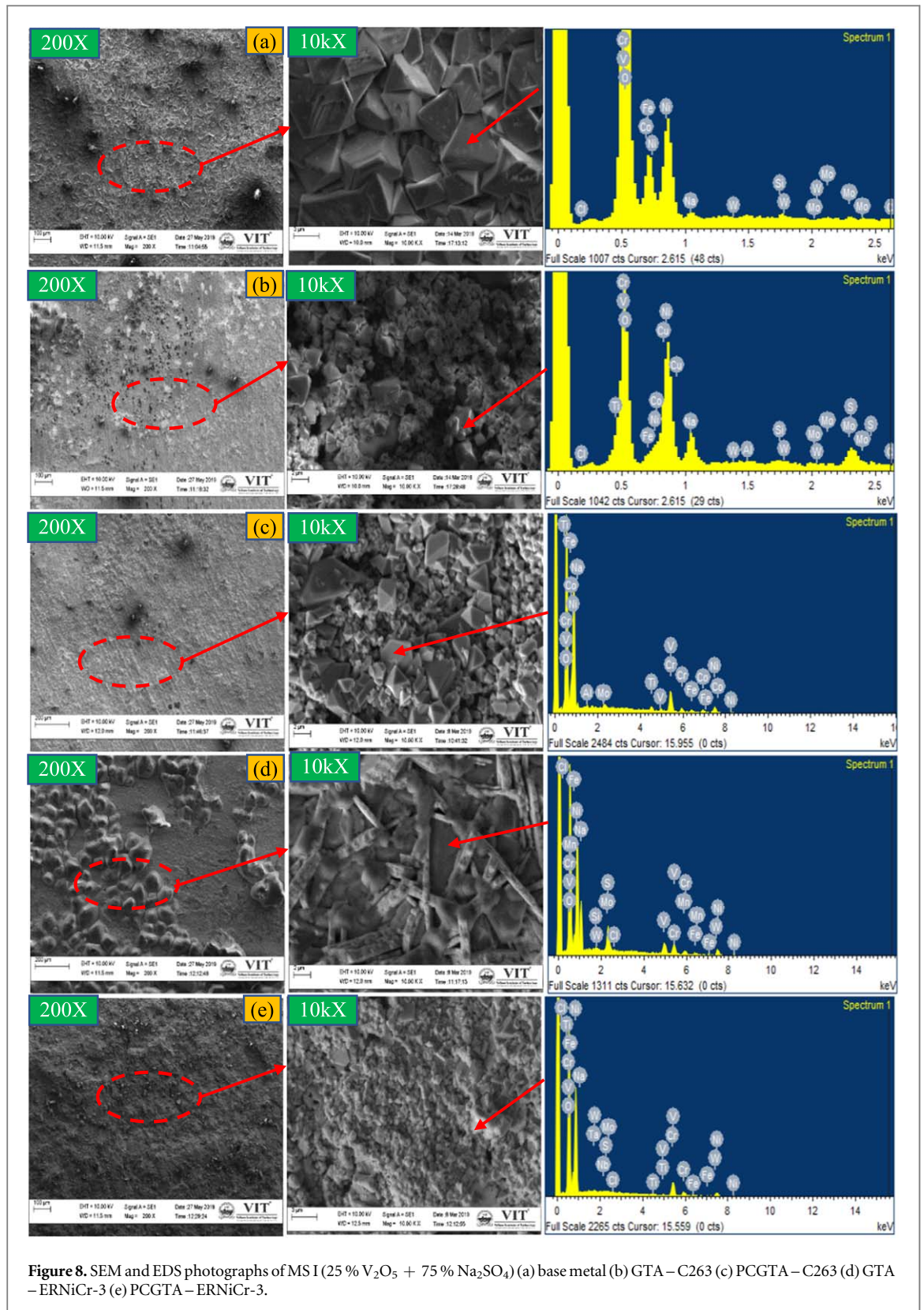


Figure 7. Corrosion kinetic curve of number of cycles for MS II (5% NaCl + 25% V<sub>2</sub>O<sub>5</sub> + 70% Na<sub>2</sub>SO<sub>4</sub>) versus WGS per surface area.

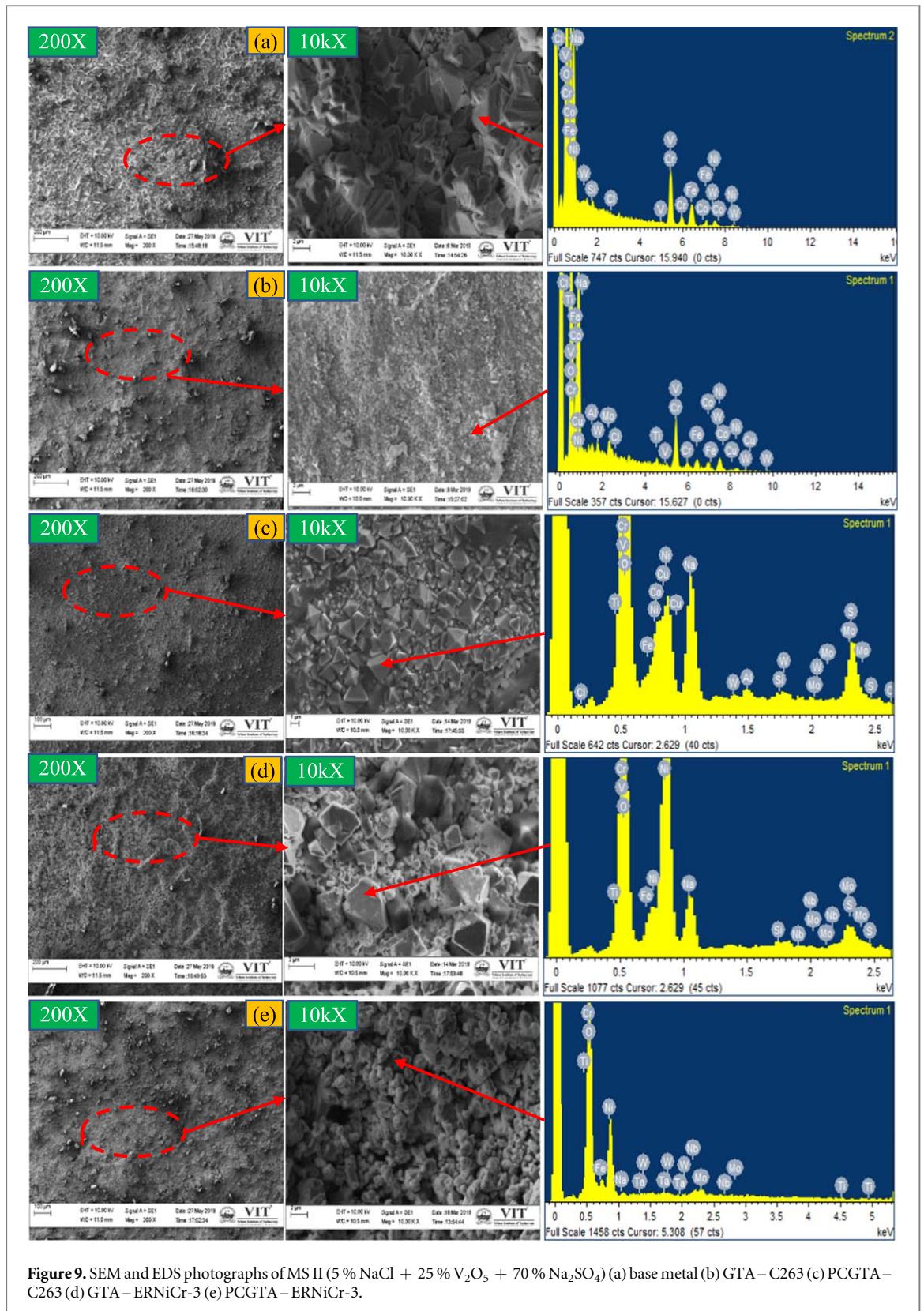
Table 3. Parabolic constant ( $K_p$ ) of hot corrosion specimens.

Type of salt	Specimen	$K_p$ value ( $\text{mg}^2/(\text{cm}^4 \cdot \text{s})$ )
MSI	Base metal	$0.218 \times 10^{-6}$
	GTA with C263 filler	$1.151 \times 10^{-6}$
	PCGTA with C263 filler	$0.008 \times 10^{-6}$
	GTA with ERNiCr-3 filler	$4.156 \times 10^{-6}$
	PCGTA with ERNiCr-3 filler	$0.003 \times 10^{-6}$
MS II	Base metal	$4.628 \times 10^{-6}$
	GTA with C263 filler	$19.900 \times 10^{-6}$
	PCGTA with C263 filler	$0.749 \times 10^{-6}$
	GTA with ERNiCr-3 filler	$21.440 \times 10^{-6}$
	PCGTA with ERNiCr-3 filler	$3.090 \times 10^{-6}$





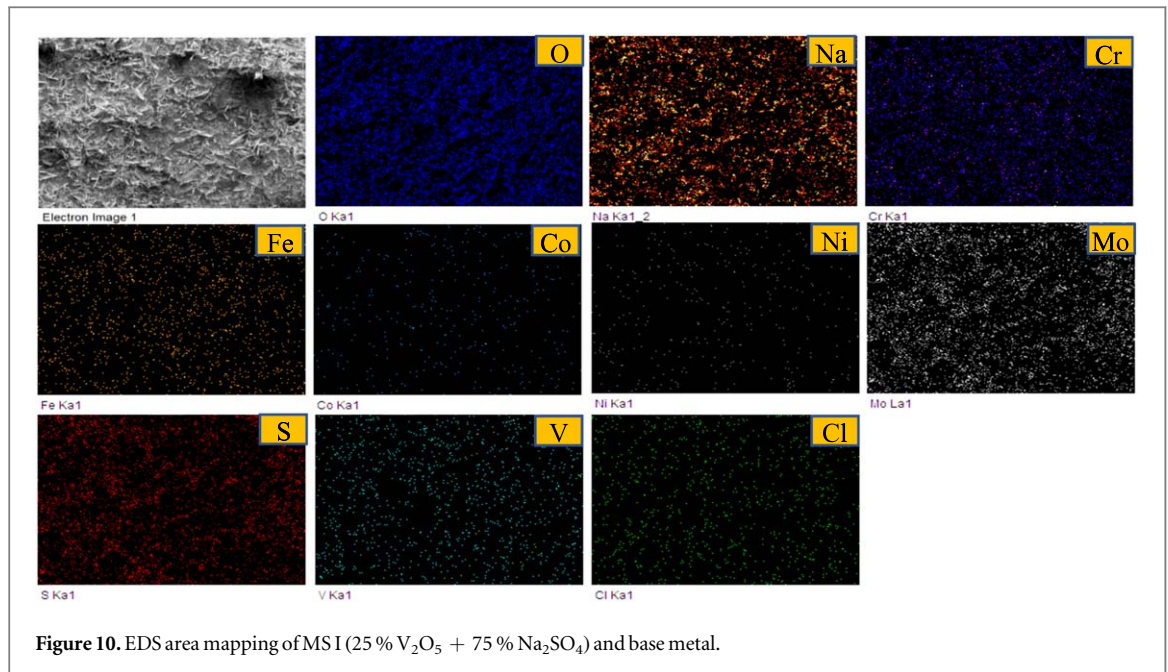
NaCl salt in the mixture of MSI is the reason for better corrosion resistance [13]. The drastic increase in weight gain square (WGS) curve and weight gain curve is observed until the 3rd cycle due to the rapid oxidation of Ni and Cr on the substrate surface and gradually increases. In MSI, GTA ERNiCr-3 showed the highest weight gain, followed by GTA C263, PCGTA C263, and PCGTA ERNiCr-3. The formation of high accelerated oxides Fe, Mo, S, V, Na in GTA causes higher weight gain for both fillers. Whereas in the case of PCGTA, the formation of more Ni, Cr, and Al oxides showed lesser weight gain and better corrosion resistance for C263 and ERNiCr-3 fillers.



Similarly, for MS II, the highest weight gain is observed for GTA with ERNiCr-3 filler followed by GTA with C263 filler, PCGTA with C263 filler, and PCGTA with ERNiCr-3 filler.

Figures 6 and 7 show the WGS and number of cycles graphs of the coated samples welded by PCGTA and GTA using C263 and ERNiCr-3 fillers. The parabolic constant is determined to identify the corrosion rate from the following equation (1) [23, 32].



**Table 4.** EDS analysis of MS I coated weldments (wt %) and base metal.

Specimens	O	Na	Cr	Fe	Ni	Mo	Co	Al	Ti	Nb	S	V
Hastelloy X	22.64	0.43	26.39	25.95	21.15	0.39	1.26	—	—	—	0.22	1.35
GTA with C263 filler	32.85	3.48	11.28	6.70	36.55	2.26	0.60	0.08	1.81	—	1.96	1.86
PCGTA with C263 filler	23.81	0.83	18.42	2.23	44.10	1.18	5.08	0.17	2.07	—	0.30	1.12
GTA with ERNiCr-3 filler	31.69	6.63	9.55	6.35	37.58	3.04	—	—	0.20	0.18	2.66	1.42
PCGTA with ERNiCr-3 filler	22.64	0.25	20.88	4.60	50.09	0.27	—	—	0.05	0.41	0.07	0.20

**Table 5.** EDS analysis of MS II coated weldments (wt %) and base metal.

Specimens	O	Na	Cr	Fe	Ni	Mo	Co	Al	Ti	Nb	S	V
Hastelloy X	24.69	0.60	22.94	27.09	23.28	0.16	0.07	—	—	—	0.05	0.11
GTA C263	23.00	2.41	16.74	11.65	31.67	4.14	5.33	0.34	1.14	—	3.21	0.14
PCGTA C263	31.07	1.34	23.77	4.44	23.79	0.71	7.88	0.31	2.91	—	0.46	1.88
GTA ERNiCr-3	28.59	4.42	8.89	9.85	37.28	4.29	—	—	0.26	0.79	4.30	1.11
PCGTA ERNiCr-3	29.36	3.39	27.13	6.50	28.03	1.76	—	—	0.34	1.73	0.32	0.45

$$\left(\frac{\Delta w}{S_A}\right)^2 = K_p \times t \quad (1)$$

whereas  $K_p$ —parabolic constant in  $\text{mg}^2 (\text{cm}^4 \cdot \text{s})^{-1}$ ,  $S_A$ —the surface area of the substrate in  $\text{cm}^2$ ,  $\Delta w$ —pre and post weight difference of the substrate (mg),  $t$ —time taken (s). Table 3 shows the parabolic constant value for the coated samples (MS I and MS II). There comes a gradual increase in WGS after the 3rd cycle due to continuous oxidation of Mo, Fe, S, Cr, V, and Na. During hot corrosion testing, the sudden reduction in the WGS of some substrates is observed in figures 6 and 7 because Cr and Na elements evaporated at 900 °C. In MS I, GTA with ERNiCr-3 filler exhibits maximum WGS per unit area trailed by GTA with C263 filler, PCGTA with C263 filler, and PCGTA with ERNiCr-3 filler. For MS II, the highest WGS is obtained in GTA with ERNiCr-3 filler followed by GTA with C263 filler, PCGTA with C263 filler, and PCGTA with ERNiCr-3 filler.

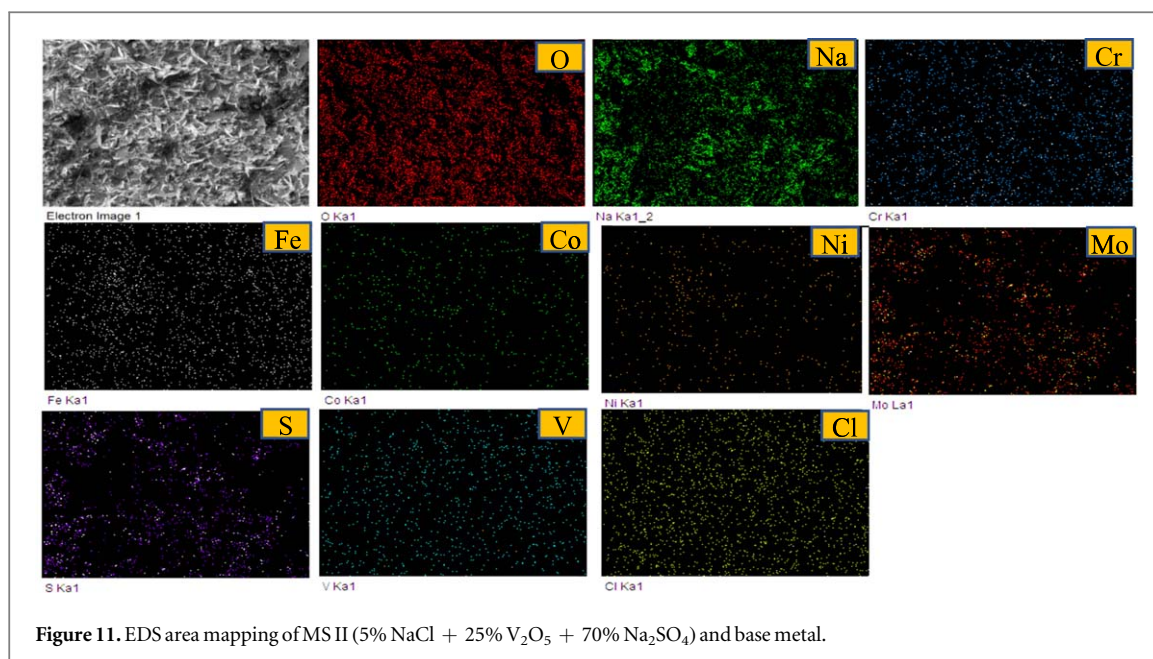
The resistance to corrosion of GTA and PCGTA weldments coated with MS I at 900 °C for both the filler materials is given by,

$$GTA\ ERNiCr - 3 < GTA\ C263 < PCGTA\ C263 \leq PCGTA\ ERNiCr - 3\ (MS\ I)$$

The corrosion resistance for GTA and PCGTA substrate with C263 and ERNiCr-3 filler wires tested at 900 °C for 250 h and coated using MS II is given below,

$$GTA\ ERNiCr - 3 < GTA\ C263 < PCGTA\ ERNiCr - 3 < PCGTA\ C263\ (MS\ II)$$





### 3.3. SEM/EDS study

The surface morphology of the substrate is identified through SEM photographs. EDS analysis determined the presence of protective and corrosive phases through the elemental percentage on the surface. The SEM/EDS photographs of GTA and PCGTA weldment with MS I and MS II coating are illustrated in figures 8(a)–(e) and 9(a)–(e). The MS I and MS II EDS point analyses are given in tables 4 and 5. In the MS I & MS II condition, the base metal shows similar major elements like Fe, O, Ni, Cr, and S, Co, V, Mo, and Na as minor elements. The availability of these elements is confirmed in EDS area mapping images (figures 10 and 11).

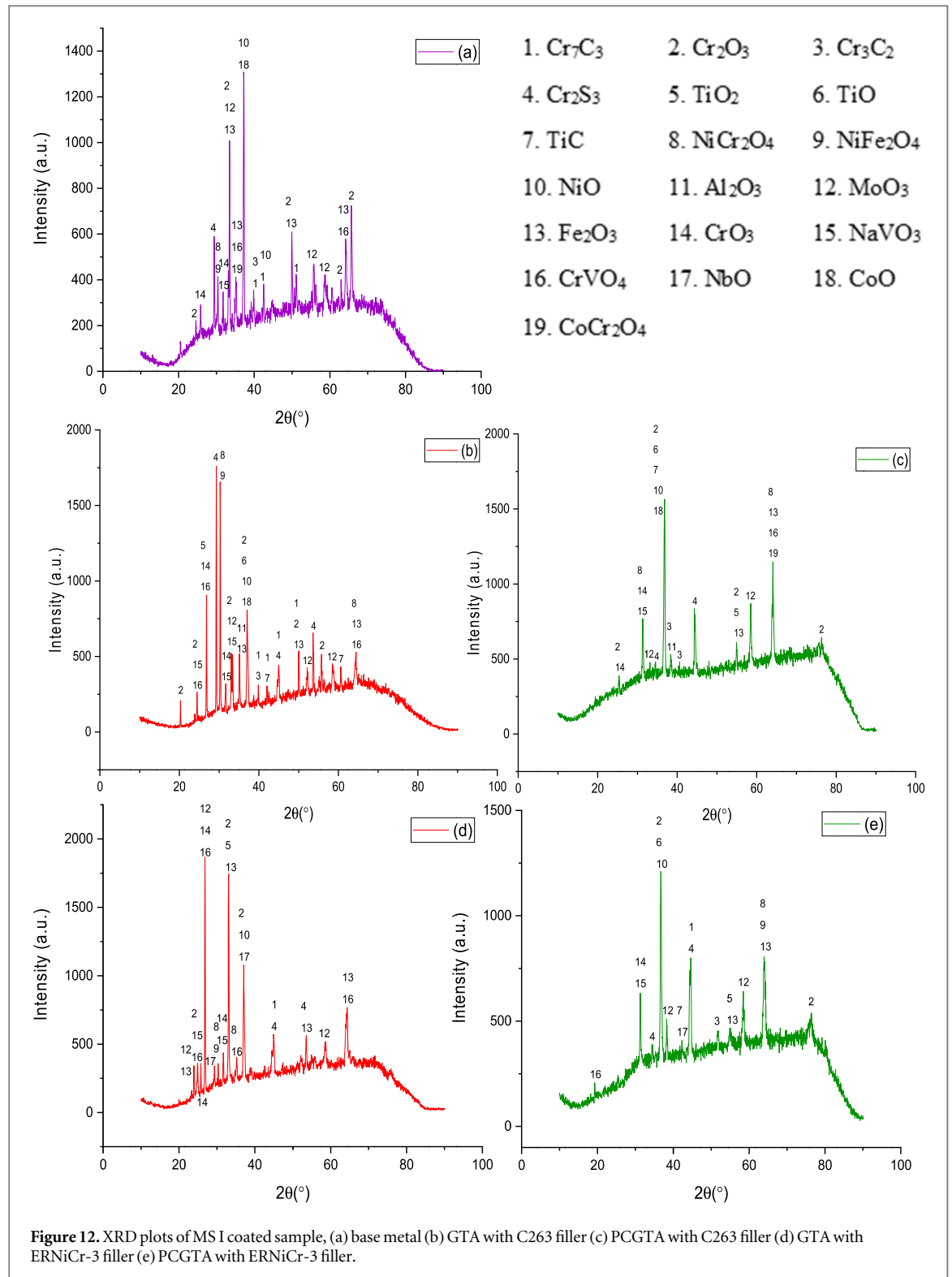
### 3.4. XRD analysis

The corrosive and protective phases on the weldment coated with MS I and MS II and base metal are evaluated through the XRD test. The phases present on the weldments and base metal after the 50th cycle are displayed in figures 12 and 13. Table 6 shows the consolidated phases of all the MS I and MS II substrates. In MS I condition, base metal shows the major phases of MoO<sub>3</sub>, NiO, Cr<sub>2</sub>O<sub>3</sub>, Fe<sub>2</sub>O<sub>3</sub>, and minor phases of NaVO<sub>3</sub>, CrO<sub>3</sub>, NiCr<sub>2</sub>O<sub>4</sub>, CoO, CoCr<sub>2</sub>O<sub>4</sub>, CrVO<sub>4</sub>, NiFe<sub>2</sub>O<sub>4</sub>, Cr<sub>3</sub>C<sub>2</sub>, Cr<sub>7</sub>C<sub>3</sub>. In MS II condition, base metal reveals Cr<sub>2</sub>O<sub>3</sub>, NiCr<sub>2</sub>O<sub>4</sub>, NiO as major phases and Cr<sub>7</sub>C<sub>3</sub>, Fe<sub>2</sub>O<sub>3</sub>, CrVO<sub>4</sub>, CoO, CrO<sub>3</sub>, NaVO<sub>3</sub>, Cr<sub>2</sub>S<sub>3</sub>, MoO<sub>3</sub> as minor phases.

In PCGTA MS I substrate, grains and grain boundaries increase a more significant number of protective phases than GTA substrate. In PCGTA C263 and ERNiCr-3, the protective phases like CoCr<sub>2</sub>O<sub>4</sub>, Cr<sub>2</sub>O<sub>3</sub>, Al<sub>2</sub>O<sub>3</sub>, NiO, NiCr<sub>2</sub>O<sub>4</sub>, and Cr<sub>2</sub>O<sub>3</sub>, NiO, NiCr<sub>2</sub>O<sub>4</sub>, NiFe<sub>2</sub>O<sub>4</sub>, NbO are obtained, respectively. This reduces the sub-surface elemental oxidation [22, 33]. The lower amount of MoO<sub>3</sub>, Fe<sub>2</sub>O<sub>3</sub>, Cr<sub>2</sub>S<sub>3</sub> as non-protective phases in PCGTA substrates reduces the weight gain. The lesser protective phases like NiFe<sub>2</sub>O<sub>4</sub>, Cr<sub>2</sub>O<sub>3</sub>, NiCr<sub>2</sub>O<sub>4</sub>, in GTA C263, and NiO, NbO, NiCr<sub>2</sub>O<sub>4</sub>, Cr<sub>2</sub>O<sub>3</sub>, NiFe<sub>2</sub>O<sub>4</sub> in GTA ERNiCr-3, are improving the weight gain (figures 4 and 5). Also, the presence of Cr<sub>2</sub>S<sub>3</sub>, MoO<sub>3</sub>, Fe<sub>2</sub>O<sub>3</sub> in GTA C263 and GTA ERNiCr-3 as the non-protective layer has improved the weight gain of substrates. The existence of O, Cr, Ni, Fe in SEM (figure 8) and EDS analysis are supported by the XRD results (figure 12) for both GTA and PCGTA substrate in MS I condition.

In PCGTA MS II substrate, the higher crystalline grain refinement provides better corrosion than GTA for both the filler materials (C263, ERNiCr-3). MS II has a higher rate of corrosion than MS I. This is due to the presence of NaCl in MS II accelerates corrosion, whereas NaCl is not included in the mixture of MS I [34]. In PCGTA C263, the more protective phases of Cr<sub>2</sub>O<sub>3</sub>, NiO, NiCr<sub>2</sub>O<sub>4</sub>, CoCr<sub>2</sub>O<sub>4</sub>, Al<sub>2</sub>O<sub>3</sub>, whereas, Cr<sub>2</sub>O<sub>3</sub>, NiO, NiCr<sub>2</sub>O<sub>4</sub>, NiFe<sub>2</sub>O<sub>4</sub>, NbO phases are observed in PCGTA ERNiCr-3. Also, a lesser non-protective phase of Fe<sub>2</sub>O<sub>3</sub>, Cr<sub>2</sub>S<sub>3</sub>, MoO<sub>3</sub> in PCGTA C263 and ERNiCr-3 substrate provided better corrosion resistance with the slight increase in weight gain WGS of PCGTA substrate, and graphs follow the parabolic law (figures 6 and 7). The larger grains in GTA substrate gives less protective phases Cr<sub>2</sub>O<sub>3</sub>, NiO, NiCr<sub>2</sub>O<sub>4</sub>, CoCr<sub>2</sub>O<sub>4</sub>, Al<sub>2</sub>O<sub>3</sub> in GTA C263 and Cr<sub>2</sub>O<sub>3</sub>, NiO, NiCr<sub>2</sub>O<sub>4</sub>, NiFe<sub>2</sub>O<sub>4</sub>, NbO in GTA ERNiCr-3 substrate with non-protective phases like Fe<sub>2</sub>O<sub>3</sub>, MoO<sub>3</sub>, Cr<sub>2</sub>S<sub>3</sub>, in both GTA substrate which in turn improves the WGS and weight gain graphs (figures 6 and 7).

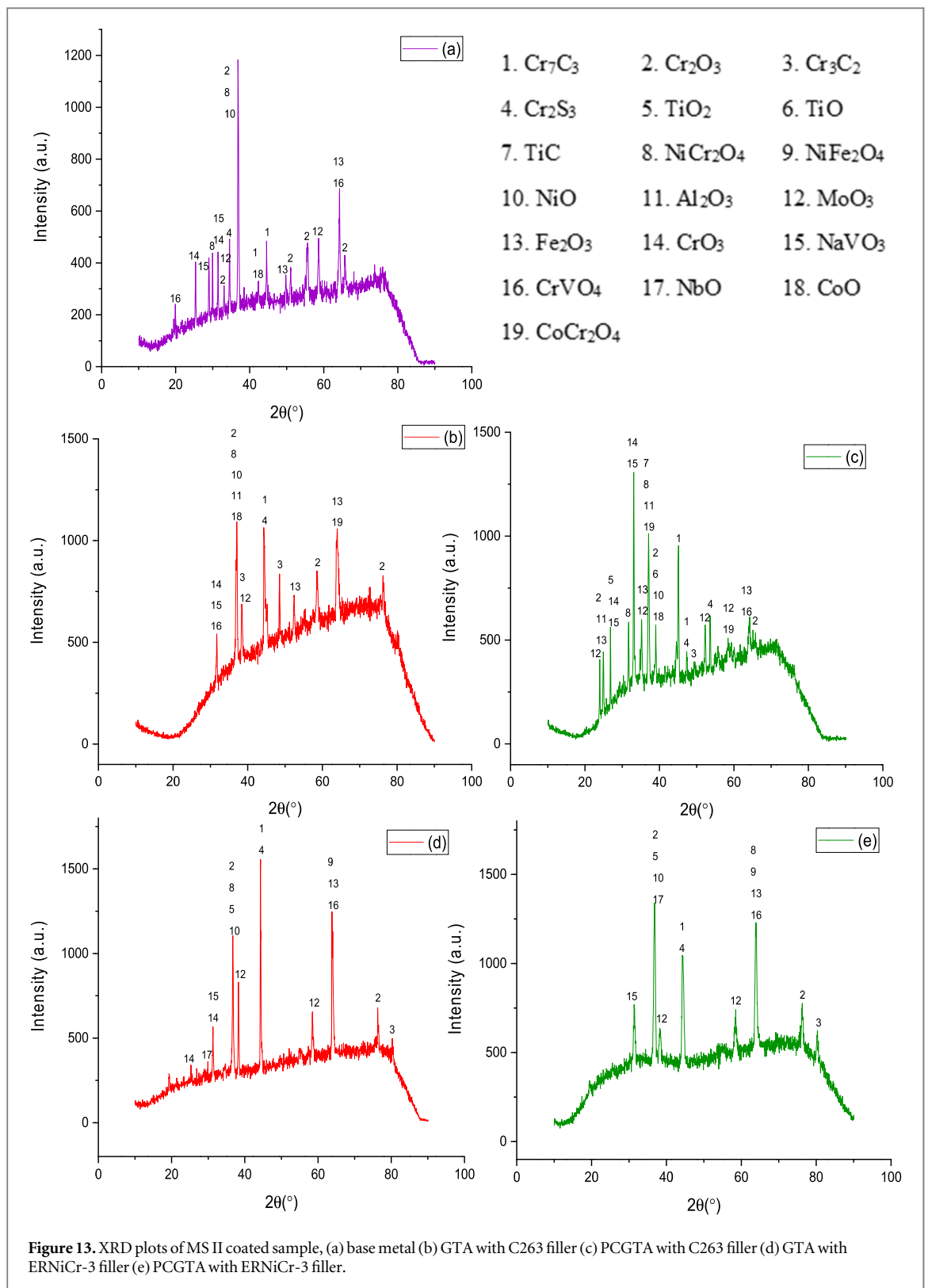
The crystalline grain size for PCGTA and GTA weldments for both C263 and ERNiCr-3 filler wires is evaluated through Scherer's formula using the Gaussian method XRD test. The PCGTA shows the crystalline grain size of 26 nm and 22 nm, whereas GTA reveals the crystalline grain size of 30 nm and 24 nm for C263 and



ERNiCr-3 filler wires, respectively. The refined grains in PCGTA show a 7.64% and 13.52% reduction in grain size compared to GTA for ERNiCr-3 and C263 filler wires. Scherer's formula for evaluating the grain size is given by (2) [24].

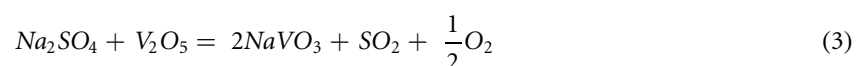
$$s = \frac{k\lambda}{\beta \cos \theta} \text{ (nm)} \quad (2)$$

where,  $k$ —dimensionless shape factor (0.94),  $\beta$ —full width half maximum (FWHM) (radian),  $\lambda$  - x-ray wavelength ( $1.54 \times 10^{-10}$  m) (m),  $s$ —mean ordered (crystalline) grain size (nm),  $\theta$ —diffraction angle (degree).



### 3.5. Chemical reactions

The  $V_2O_5$  and  $Na_2SO_4$  salt mixture reacts and forms the  $NaVO_3$  oxides during the initial stages of hot corrosion testing [35]. This  $NaVO_3$  oxide is the reason for the rapid oxidation of the initial few cycles and drastically increases the substrate's weight gain. The reaction of salts is given in the below equation (3) [13, 35].



The  $NiO$  and  $Cr_2O_3$  are formed as the product of a reaction between  $Ni$  and  $Cr$  with  $O$  during hot corrosion testing, and this acts as a diffusion barrier to oxidation through other elements [36]. The gradual improvement



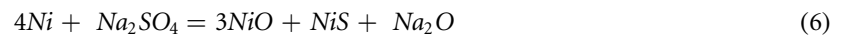
**Table 6.** XRD analysis of MS I and MS II coated weldments (wt %) and base metal.

Salt	Samples	Major phase	Minor phase
MSI	Base metal	MoO <sub>3</sub> , NiO, Cr <sub>2</sub> O <sub>3</sub> , Fe <sub>2</sub> O <sub>3</sub> ,	CrO <sub>3</sub> , NiCr <sub>2</sub> O <sub>4</sub> , NaVO <sub>3</sub> , CoO, CoCr <sub>2</sub> O <sub>4</sub> , NiFe <sub>2</sub> O <sub>4</sub> , CrVO <sub>4</sub> , Cr <sub>3</sub> C <sub>2</sub> , Cr <sub>7</sub> C <sub>3</sub>
	GTA with C263 filler	NiCr <sub>2</sub> O <sub>4</sub> , Cr <sub>2</sub> O <sub>3</sub> , TiO, Cr <sub>2</sub> S <sub>3</sub> , TiO <sub>2</sub> , CrO <sub>3</sub> , CrVO <sub>4</sub> , NiFe <sub>2</sub> O <sub>4</sub>	MoO <sub>3</sub> , NaVO <sub>3</sub> , Al <sub>2</sub> O <sub>3</sub> , Fe <sub>2</sub> O <sub>3</sub> , Cr <sub>7</sub> C <sub>3</sub> , Cr <sub>3</sub> C <sub>2</sub> , TiC, CoO
	PCGTA with C263 filler	Cr <sub>2</sub> O <sub>3</sub> , TiO, TiC, NiCr <sub>2</sub> O <sub>4</sub> , NiO, CrO <sub>3</sub> , CoO, CoCr <sub>2</sub> O <sub>4</sub>	MoO <sub>3</sub> , NaVO <sub>3</sub> , Al <sub>2</sub> O <sub>3</sub> , Fe <sub>2</sub> O <sub>3</sub> , Cr <sub>3</sub> C <sub>2</sub> , TiO <sub>2</sub> , CrVO <sub>4</sub> , Cr <sub>2</sub> S <sub>3</sub>
	GTA with ERNiCr-3 filler	Cr <sub>2</sub> O <sub>3</sub> , TiO <sub>2</sub> , NiO, MoO <sub>3</sub> , CrO <sub>3</sub> , CrVO <sub>4</sub> , NbO	Fe <sub>2</sub> O <sub>3</sub> , NaVO <sub>3</sub> , NiCr <sub>2</sub> O <sub>4</sub> , NiFe <sub>2</sub> O <sub>4</sub> , Cr <sub>7</sub> C <sub>3</sub> , Cr <sub>2</sub> S <sub>3</sub>
	PCGTA with ERNiCr-3 filler	Cr <sub>2</sub> O <sub>3</sub> , TiO, NiO, NiCr <sub>2</sub> O <sub>4</sub> , NiFe <sub>2</sub> O <sub>4</sub>	Fe <sub>2</sub> O <sub>3</sub> , NaVO <sub>3</sub> , CrVO <sub>4</sub> , CrO <sub>3</sub> , MoO <sub>3</sub> , TiC, NbO, Cr <sub>7</sub> C <sub>3</sub> , Cr <sub>2</sub> S <sub>3</sub> , TiO <sub>2</sub>
MSII	Base metal	Cr <sub>2</sub> O <sub>3</sub> , NiO, NiCr <sub>2</sub> O <sub>4</sub>	CrVO <sub>4</sub> , CrO <sub>3</sub> , NaVO <sub>3</sub> , Cr <sub>2</sub> S <sub>3</sub> , Cr <sub>7</sub> C <sub>3</sub> , Fe <sub>2</sub> O <sub>3</sub> , MoO <sub>3</sub> , CoO
	GTA with C263 filler	Cr <sub>2</sub> O <sub>3</sub> , NiO, NiCr <sub>2</sub> O <sub>4</sub> , Cr <sub>2</sub> S <sub>3</sub> , Fe <sub>2</sub> O <sub>3</sub> , Cr <sub>7</sub> C <sub>3</sub> , CoO, CoCr <sub>2</sub> O <sub>4</sub>	MoO <sub>3</sub> , NaVO <sub>3</sub> , CrVO <sub>4</sub> , CrO <sub>3</sub> , Cr <sub>3</sub> C <sub>2</sub> , Al <sub>2</sub> O <sub>3</sub>
	PCGTA with C263 filler	Cr <sub>2</sub> O <sub>3</sub> , NiO, NiCr <sub>2</sub> O <sub>4</sub> , Fe <sub>2</sub> O <sub>3</sub> , NaVO <sub>3</sub> , Cr <sub>7</sub> C <sub>3</sub> , CoO, CoCr <sub>2</sub> O <sub>4</sub>	MoO <sub>3</sub> , Al <sub>2</sub> O <sub>3</sub> , TiO <sub>2</sub> , TiC, TiO, Cr <sub>3</sub> C <sub>2</sub> , Cr <sub>2</sub> S <sub>3</sub> , CrVO <sub>4</sub>
	GTA with ERNiCr-3 filler	Cr <sub>2</sub> O <sub>3</sub> , NiO, NiCr <sub>2</sub> O <sub>4</sub> , NiFe <sub>2</sub> O <sub>4</sub> , TiO <sub>2</sub> , Fe <sub>2</sub> O <sub>3</sub> , CrVO <sub>4</sub> , Cr <sub>7</sub> C <sub>3</sub> , Cr <sub>2</sub> S <sub>3</sub>	MoO <sub>3</sub> , NaVO <sub>3</sub> , CrO <sub>3</sub> , NbO, Cr <sub>3</sub> C <sub>2</sub>
	PCGTA with ERNiCr-3 filler	Cr <sub>2</sub> O <sub>3</sub> , NiO, NiCr <sub>2</sub> O <sub>4</sub> , NiFe <sub>2</sub> O <sub>4</sub> , TiO <sub>2</sub> , Fe <sub>2</sub> O <sub>3</sub> , CrVO <sub>4</sub> , Cr <sub>7</sub> C <sub>3</sub>	MoO <sub>3</sub> , NaVO <sub>3</sub> , NbO, Cr <sub>2</sub> S <sub>3</sub>

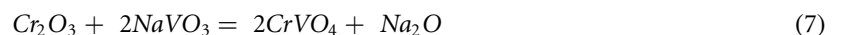
in WGS rate and weight gain follows the parabolic law [35, 37]. The more amount of Cr in all MS I and MS II substrates is confirmed by EDS analysis [16]. The chemical reactions of Ni, Cr, O during initial cycles are given in the below equations (4) and (5) [33].



The presence of Na<sub>2</sub>SO<sub>4</sub> salt also reacts with Ni and forms the NiO, NiS, and Na<sub>2</sub>O. This reaction is given in the below equation (6) [13, 38].



The reaction of Na<sub>2</sub>SO<sub>4</sub> and Cr<sub>2</sub>O<sub>3</sub> forms the CrVO<sub>4</sub> oxides, and this oxide is not protecting the substrate from oxidation. The formation of oxides creates the Cr<sub>2</sub>O<sub>3</sub> dissolution in most places and causes Cr depletion, further improving the corrosion rate. Due to this, most of the region of substrate pores are started forming, which improves the weight gain of the substrate, and reaction is given in equation (7) [13].



The presence of Cr<sub>2</sub>O<sub>3</sub>, NiO, and Fe<sub>2</sub>O<sub>3</sub>, NiO, is reacted with each other and forms the NiCr<sub>2</sub>O<sub>4</sub> and NiFe<sub>2</sub>O<sub>4</sub> spinel oxides, providing the protective layer to the substrate for further corrosion. The anions and cations diffusion co-efficient for the spinel oxides is much lower than other oxides and forms more protection for all the substrates at high temperatures. The higher corrosion resistance in PCGTA weldments is due to the refined grain structure and spinel oxides' presence. The equations (8) and (9) for the formation of spinel oxides are given below [13, 17].



The development of Cr<sub>2</sub>S<sub>3</sub> is found at the molten salt coating and weldment interface region. This improves the corrosion rate of the substrate by destroying the alloying elements. It also forms Cr<sub>2</sub>O<sub>3</sub> by reacting with oxygen, and the equation (10) is given by [14, 39].



The MoO<sub>3</sub> and Fe<sub>2</sub>O<sub>3</sub> (non-protective phases) on the substrate cause alloying elements acid fluxing, promoting spallation, chipping, exfoliation of oxide scale, and cracking. This increases the substrate weight gain while reacting with the sub-surface [40].

## 4. Conclusions


In the present study, the high-temperature corrosion behavior of GTA and PCGTA welded Hastelloy X with C263 and ERNiCr-3 in MS I and MS II environments are studied, and its results are as follows:

1. The MS II coated substrate at 900 °C for 50 cycles shows the highest weight gain for all the PCGTA and GTA weldment joined using C263 and ERNiCr-3 filler wires to MS I coated substrates.
2. The change of color in each cycle depicts the occurrence of hot corrosion in both GTA and PCGTA weldments coated with MS I and MS II. The parabolic constant for GTA ERNiCr-3 coated with MS II showed the highest value of  $21.440 \times 10^{-6} \text{ mg}^2/(\text{cm}^4 \cdot \text{s})$ . The MS I coated PCGTA C263 weldment, revealed the parabolic constant of  $0.008 \times 10^{-6} \text{ mg}^2/(\text{cm}^4 \cdot \text{s})$  (lowest).
3. The resistance against hot corrosion of MS I and MS II coated substrates in the increasing pattern is GTA ERNiCr-3 < GTA C263 < PCGTA ERNiCr-3 < PCGTA C263.
4. In MS I and MS II, the crystalline grain refinement observed for C263 and ERNiCr-3 fillers causes more grain boundaries and grains in the substrate, which develops more protective phases and better corrosion resistance in PCGTA than GTA.
5. The protective phases of Cr<sub>2</sub>O<sub>3</sub>, NiO, NiCr<sub>2</sub>O<sub>4</sub>, CoCr<sub>2</sub>O<sub>4</sub>, Al<sub>2</sub>O<sub>3</sub>, NiFe<sub>2</sub>O<sub>4</sub>, and NbO are responsible for better corrosion resistance. The phases like Fe<sub>2</sub>O<sub>3</sub>, MoO<sub>3</sub>, and Cr<sub>2</sub>S<sub>3</sub>, which act as the non-protective phase, decrease corrosion resistance. These phases cause acid fluxing of alloying elements, which promote the spallation, chipping, exfoliation of oxide scale, and cracking.
6. Based on the chosen welding conditions, PCGTA C263 weldment with MS I and MS II coating shows excellent corrosion resistance. Hence, it is recommended for welding aerospace components like thrust reverser and combustion chamber, which are operated at higher temperatures when compared to ERNiCr weldments.

## Acknowledgments

The authors thank Vellore Institute of Technology (VIT) Vellore for the support to perform a hot corrosion study using SEM/EDS, XRD instruments to perform this work.

## ORCID iDs

M Sathishkumar  <https://orcid.org/0000-0003-0726-8731>  
M Manikandan  <https://orcid.org/0000-0002-4467-1493>  
B Arulmurugan  <https://orcid.org/0000-0001-7143-3653>  
Senthil Kumar Selvaraj  <https://orcid.org/0000-0001-9994-9424>  
M Vignesh  <https://orcid.org/0000-0001-7552-3154>  
S Rajakumar  <https://orcid.org/0000-0001-8011-4961>  
S Rajkumar  <https://orcid.org/0000-0002-6544-3852>

## References

- [1] Hetmanczyk M, Swadzba L and Mendala B 2007 Advanced materials and protective coatings in aero-engines application co-operating with Manufacturing and processing *J Achiev Mater Manuf. Eng.* **24** 372–81
- [2] Stringer J 2016 High-temperature corrosion of superalloys *Mater. Sci. Technol.* **3** 482–93
- [3] Stephen Leon J, Bharathiraja G and Jayakumar V 2020 Experimental and numerical investigations of optimum process window for friction stir welding using flat faced tool pin *Indian J. Sci. Technol.* **13** 2609–25
- [4] Stephen Leon J, Bharathiraja G and Jayakumar V 2020 A review on friction stir welding in aluminium alloys *IOP Conf. Ser.: Mater. Sci. Eng.* **954** 012007
- [5] Inconel alloy HX (UNSN06002) 2005 Special Metal Corporation Technical data sheet <http://specialmetals.com/assets/smc/documents/alloys/inconel/inconel-alloy-hx.pdf>
- [6] Sathishkumar M et al 2020 Investigation of double-pulsed gas metal arc welding technique to preclude carbide precipitates in aerospace grade hastelloy x *J. Mater. Eng. Perform.* **30** 661–84
- [7] Sathishkumar M and Manikandan M 2020 Development of pulsed current arc welding to preclude carbide precipitates in hastelloy x weldment using ERNiCr-3 *J. Mater. Eng. Perform.* **29** 5395–408
- [8] Sathishkumar M and Manikandan M 2019 Hot corrosion behaviour of continuous and pulsed current gas tungsten arc welded hastelloy x in different molten salts environment *Mater. Res. Express* **6** 126553

- [9] Wang X et al 2017 Control of precipitation behaviour of hastelloy-X through grain boundary engineering *Mater. Sci. Technol.* **33** 2078–85
- [10] Shifler D A 2018 Hot corrosion: a modification of reactants causing degradation *Mater. High Temp.* **35** 225–35
- [11] Sumner J, Potter A, Simms N J and Oakey J E 2015 Hot corrosion resistance of gas turbine materials in combusted syngas environments *Mater. High Temp.* **32** 177–87
- [12] Eliaz N, Shemesh G and Latanision R 2002 Hot corrosion in gas turbines *Eng. Fail. Anal.* **9** 31–43
- [13] Salehi Doolabi M, Ghasemi B, Sadrnezhaad S K, Habibollahzadeh A and Jafarzadeh K 2017 Hot corrosion behavior and near-surface microstructure of a 'low-temperature high-activity Cr-aluminide' coating on inconel 738LC exposed to  $\text{Na}_2\text{SO}_4$ ,  $\text{Na}_2\text{SO}_4 + \text{V}_2\text{O}_5$  and  $\text{Na}_2\text{SO}_4 + \text{V}_2\text{O}_5 + \text{NaCl}$  at 900 °C *Corros. Sci.* **128** 42–53
- [14] Guangyan F, Zeyan Q, Jingyu C, Qun L and Yong S 2015 Hot corrosion behavior of Ni-base alloys coated with salt film of 75% $\text{Na}_2\text{SO}_4 + 25\%\text{NaCl}$  at 900 °C *Rare Met. Mater. Eng.* **44** 1112–5
- [15] Chellaganesh D, Khan M A and Jappes J T W 2019 High temperature oxidation behavior of thermally sprayed alumina—titania coatings on nickel based superalloys *Mater. Res. Express* **6** 86521
- [16] Choi H M et al 1998 Effect of the thickness of plasma-sprayed coating on bond strength and thermal fatigue characteristics *J. Mater. Sci.* **33** 5895–9
- [17] Singh H, Puri D, Prakash S and Maiti R 2007 Characterization of oxide scales to evaluate high temperature oxidation behavior of Ni-20Cr coated superalloys *Mater. Sci. Eng. A* **464** 110–6
- [18] Hari P R, Arivazhagan N, Rao M N and Pavan A H V 2019 High temperature corrosion of alloy 617 OCC at 700 °C in simulated USC power plant environment *Mater. Res. Express* **6** 76557
- [19] Karimi A, Soltani R, Ghambari M and Fallahdoost H 2017 High temperature oxidation resistance of plasma sprayed and surface treated YSZ coating on Hastelloy X *Surf. Coatings. Technol.* **321** 378–85
- [20] Matsukawa C, Hayashi S, Yakuwa H, Kishikawa T, Narita T and Ukai S 2011 High-temperature carburization behaviour of HASTELLOY X in  $\text{CH}_4$  gas *Corros. Sci.* **53** 3131–8
- [21] Liu M et al 2013 Investigation on corrosion behavior of Ni-based alloys in molten fluoride salt using synchrotron radiation techniques *J. Nucl. Mater.* **440** 124–8
- [22] Somasundaram B, Kadoli R and Ramesh M 2015 Hot corrosion behaviour of HVOF sprayed ( $\text{Cr}_3\text{C}_2$ -35% NiCr) + 5% Si coatings in the presence of  $\text{Na}_2\text{SO}_4$ -60%  $\text{V}_2\text{O}_5$  at 700 °C *Trans. Indian Inst. Met.* **68** 257–68
- [23] Sreenivasulu V and Manikandan M 2018 Hot corrosion studies of HVOF sprayed carbide and metallic powder coatings on alloy 80A at 900 °C *Mater. Res. Express* **6** 36519
- [24] Sathishkumar M and Manikandan M 2019 Preclusion of carbide precipitates in the Hastelloy X weldment using the current pulsing technique *J. Manuf. Process.* **45** 9–21
- [25] Manikandan M, Arivazhagan N, Nageswara Rao M and Reddy G M 2014 Microstructure and mechanical properties of alloy C-276 weldments fabricated by continuous and pulsed current gas tungsten arc welding techniques *J. Manuf. Process* **16** 563–72
- [26] Sen M, Mukherjee M, Kumar S and Kumar T 2018 Effect of double-pulsed gas metal arc welding (DP-GMAW) process variables on microstructural constituents and hardness of low carbon steel weld deposits *J. Manuf. Process* **31** 424–39
- [27] Verma J and Taiwade R V 2017 Effect of welding processes and conditions on the microstructure, mechanical properties and corrosion resistance of duplex stainless steel weldments—a review *J. Manuf. Process* **25** 134–52
- [28] Arulmurugan B, Sathishkumar M, Balaji D, Muralikrishnan K, Pranesh S, Praveen V, Kumar P V, Arivazhagan N and Manikandan M 2021 Development of arc welding technique to preclude microsegregation in the dissimilar joint of Alloy C-2000 and C-276 *Proc. Inst. Mech. Eng. Part E J. Process Mech. Eng.* **235** 1408–19
- [29] Subramani P and Manikandan M 2018 Development of welding technique to suppress the microsegregation in the aerospace grade alloy 80A by conventional current pulsing technique *J. Manuf. Process* **34** 579–92
- [30] Wu K, Ding N, Yin T, Zeng M and Liang Z 2018 Effects of single and double pulses on microstructure and mechanical properties of weld joints during high-power double-wire GMAW *J. Manuf. Process* **35** 728–34
- [31] Bai P, Wang Z, Hu S, Ma S and Liang Y 2017 Sensing of the weld penetration at the beginning of pulsed gas metal arc welding *J. Manuf. Process* **28** 343–50
- [32] Sreenivasulu V and Manikandan M 2018 High-temperature corrosion behaviour of air plasma sprayed  $\text{Cr}_3\text{C}_2$ -25NiCr and NiCrMoNb powder coating on alloy 80A at 900 °C *Surf. Coatings. Technol.* **337** 250–9
- [33] Sreenivas K S and Radhakrishnan V M 1998 Oxidation and hot corrosion behaviour of Nimonic-75 superalloy. *Indian J. Eng. Mater. Sci.* **5** 295–301
- [34] Arivazhagan N, Singh S, Prakash S and Reddy G M 2009 Hot corrosion studies on dissimilar friction welded low alloy steel and austenitic stainless steel under chlorine containing salt deposits under cyclic conditions *Corros. Eng. Sci. Technol.* **44** 369–80
- [35] Bluni S T and Marder A R 1996 Effects of thermal spray coating composition and microstructure on coating response and substrate protection at high temperatures *Corros.* **52** 213–8
- [36] Rizhang Z, Manjiou G and Yu Z 1987 A study of the mechanism of internal sulfidation-internal oxidation during hot corrosion of Ni-base alloys *Oxid. Met.* **27** 253–65
- [37] Kaur M, Singh H and Prakash S 2012 High-temperature behavior of a high-velocity oxy-fuel sprayed  $\text{Cr}_3\text{C}_2$ -NiCr coating. *Metall. Mater. Trans. A Phys. Metall. Mater. Sci.* **43** 2979–93
- [38] Li W, Liu Y, Wang Y, Han C and Tang H 2012 Hot corrosion behavior of Ni-16Cr-xAl based alloys in mixture of  $\text{Na}_2\text{SO}_4$ -NaCl at 600 °C *Trans. Nonferrous Met. Soc. China* **21** 2617–25
- [39] Kameswari S 1986 The role of NaCl in the hot-corrosion behavior of Nimonic alloy 90 *Oxid. Met.* **26** 33–44
- [40] Bhatia R, Singh H and Sidhu B S 2014 Hot corrosion studies of HVOF-sprayed coating on T-91 boiler tube steel at different operating temperatures *J. Mater. Eng. Perform.* **23** 493–505